Oil & Natural Gas Technology

DOE Award No.: DE-FE0009897

Quarterly Research Performance Progress Report (Period ending 6/30/2016)

Hydrate-Bearing Clayey Sediments: Morphology, Physical Properties, Production and Engineering/Geological Implications

Project Period (10/1/2012 to 9/30/2017)

Submitted by:
J. Carlos Santamarina

Georgia Institute of Technology
DUNS #: 097394084
505 10th street
Atlanta , GA 30332
e-mail: jcs@gatech.edu
Phone number: (404) 894-7605

Prepared for:
United States Department of Energy
National Energy Technology Laboratory

Submission date: 7/31/2016

Office of Fossil Energy

DISCLAIMER:

ACCOMPLISHMENTS

Context – Goals. *Fine grained sediments host more than 90% of the global gas hydrate accumulations. Yet, hydrate formation in clayey sediments is least understood and characterized. This research focuses on hydrate bearing clayey sediments. The goals of this research are (1) to gain a fundamental understanding of hydrate formation and ensuing morphology, (2) to develop laboratory techniques to emulate "natural" formations, (3) to assess and develop analytical tools to predict physical properties, (4) to evaluate engineering and geological implications, and (5) to advance gas production alternatives to recover methane from these sediments.*

Accomplished

The main accomplishments for this period include:

- Gas migration in soft sediments
  - New experimental results with viscous fluids
- Critical injection pressure
  - Models and underlying theories
  - Capillarity signature through pore throats
- Hydrate formation in specimens with low water content
- Flow rate during gas production

Plan - Next reporting period

1. Advance the understanding of crystal-sediment interaction.
2. Gas Migration in Soft Sediments: Numerical analyses
3. Stiffness characterization of hydrate bearing clays (i.e., wave velocity and Poisson's ratio at various hydrate saturations)
4. Advance numerical experiments to predict properties
5. Theoretical and analytical study of gas production

RESEARCH IN PROGRESS

Gas Migration in Shallow Sediments: Viscous Fluids

Gas injection tests were conducted at different effective stress conditions (from 0.15 kPa to 44 kPa) to simulate gas migration in the sea floor in view of potential hydrate accumulations at shallow depth. Additional experimental work using viscos fluids has been conducted to compare the difference from gas injection and to gain insight into fracture like failure in marine sediments.

The injection fluid contains 70% sucrose solution, resulting in a solution with viscosity about 400 times larger than that of water. Figure 1 shows the front and left view of the inclusion. The injection also develops a fracture-like plane, similar to the injection of gas. However, the pressure-time data does not show a saw shape curve which is due to the incompressibility of the liquid.

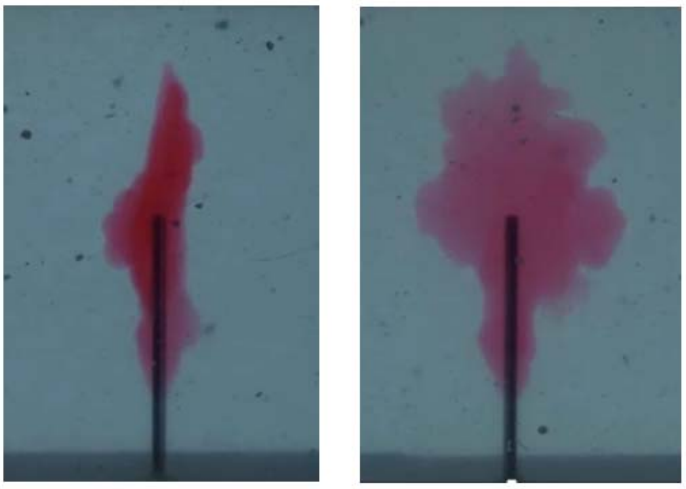

Figure 1. Front and left view of the inclusion created by 70% sucrose solution injection at σ_v = 18kPa. The red color is due to a red food dye in the sucrose solution.

The injection pressure for all tests are collected in Figure 2. The injection pressure for viscous liquid follows the same trend of gas-induced fracture-like failure (refer to the ending-March report).

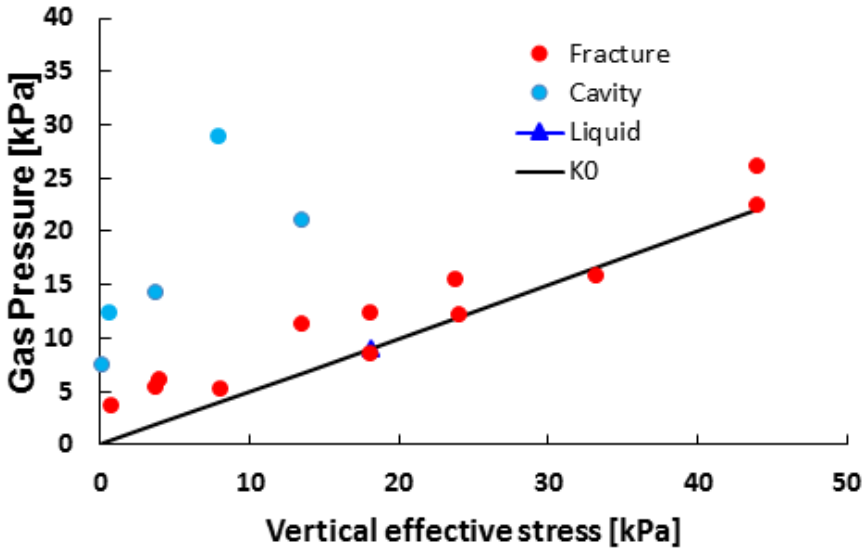

Figure 2. Fluid injection pressure versus vertical effective stress.

Critical Injection Pressure

Pressure-induced Failure. The internal pressure-induced failure in sediments is an important concern in different engineering applications, e.g. directional drilling, dam safety, hydraulic conductivity measurement, in situ remediation, grouting, and so on. The critical injection pressure which induces failure of the sediments has been studied for different purpose. Table 1 summarizes the major models for these applications and they fall into three categories based on the underlying theories: 1). Elastic solution combing different failure criteria; 2) Cavity expansion theory with different material models; 3) Linear fracture mechanics. Most models assume tensile strength, fracture toughness or apply undrained analysis (cohesive material).

However, soil is particulate in nature and its mechanical properties are effective stress-dependent. Experiments (Oppenheimer et al., 2015) and numerical simulations (Shin and Santamarina, 2010; Shin and Santamarina, 2011) have shown that fracture-like failure happens in sediments with zero tensile strength. Besides, we also observed transition from cavity to fracture-like failure at different effective stress or at different stages. Clearly an effective stress-based analysis is required to explain this phenomenon.

Table 1. Proposed models for internal pressure-induced failure in soils from the literature (cylindrical hole).

Category	Equation	Description	Reference
Cavity Expansion	$P_{ci} = \sigma_0 + s_u\left[1 + \ln\left(\frac{G}{s_u}\right)\right]$	Limit pressure of cavity expansion theory; cohesive soil	Wheeler (1990); Vesic (1972); Carter et al. (1986)
	$P_{ci} = \left(\sigma'_f + c\cdot\cot\varphi\right)\cdot\left[\left(\frac{r_0}{r_p}\right)^2 + Q\right]^{\frac{-\sin\varphi}{1+\sin\varphi}} - c\cdot\cot\varphi + u$ $\sigma'_f = \sigma'_0\left(1+\sin\varphi\right) + c\cos\varphi$ $Q = \left(\sigma'_0\sin\varphi + c\cos\varphi\right)/G$	Cavity expansion theory, Mohr-Coulomb criterion	Keulen (2001)
	$\varepsilon_{\max} = \frac{\sigma_0 + a}{2\mu}\cdot\frac{1-m}{1+m}\cdot\left(\frac{1+m}{2}\cdot\frac{P_{ci}+a}{\sigma_0+a}\right)^{\frac{k+1}{1-m}}$ $a = c\cot\varphi; m = \left(1-\sin\varphi\right)/1+\sin\varphi; k = \left(1-\sin\psi\right)/\left(1+\sin\psi\right)$	Cavity expansion theory, maximum strain criterion	Keulen (2001)
Linear Elastic Fracture Mechanics	$P_{ci} = \sigma_0 + \frac{CK_{IC}}{\sqrt{\pi a}}$	Linear elastic fracture mechanics	Murdoch (1993); Johnson et al. (2002); Barry et al. (2010); Jain and Juanes (2009)
Elastic Theory	$P_{ci} = 2\sigma_0 - u_0 + \sigma'_t$	Elasticity, tensile failure criterion	Marchi et al. (2013)
	$P_{ci} = \sigma_0 + s_u$	Elasticity, shear failure, unconsolidated undrained shear strength	Yanagisawa and Panah (1994)
Empirical formula	$P_{ci} = m\sigma_0 + \sigma_{ta}$	Empirical formula, tensile failure	Jaworski et al. (1981)
Nonlinear/ Pore Pressure Change	$P_{ci} = \sigma_0 + \Delta u$ Δu is calculated by FEM	Tensile failure	Anderson et al.. (1994)

Capillarity Signature through Pore Throats. Capillarity controls the distribution and transport of multi-phase and immiscible fluids in sediments. Capillary tube experiments are conducted to explore the propagation of fluid interfaces across pore constrictions. Measured pressure signatures reflect the interaction between surface tension, contact angle, and the pore geometry.

Various instabilities occur as the interface traverses the pore constriction, consequently, measured pressure signatures differ from theoretical trends predicted from geometry, lower capillary pressures are generated in advancing wetting fronts, and jumps are prone to under-sampling. Pressure-time P-t signatures and concurrent images are recorded for all fluids and injection rates as the liquid-gas interface traverses the tube constriction. A signature recorded during a receding test and selected snapshots are presented in Figure 3. Notice the change in capillary pressure across the pore throat, the sudden jump at point-e, the formation of a plug at the pore throat (point-f) and the associated increase in capillary pressure until a new jump takes place at point-h.

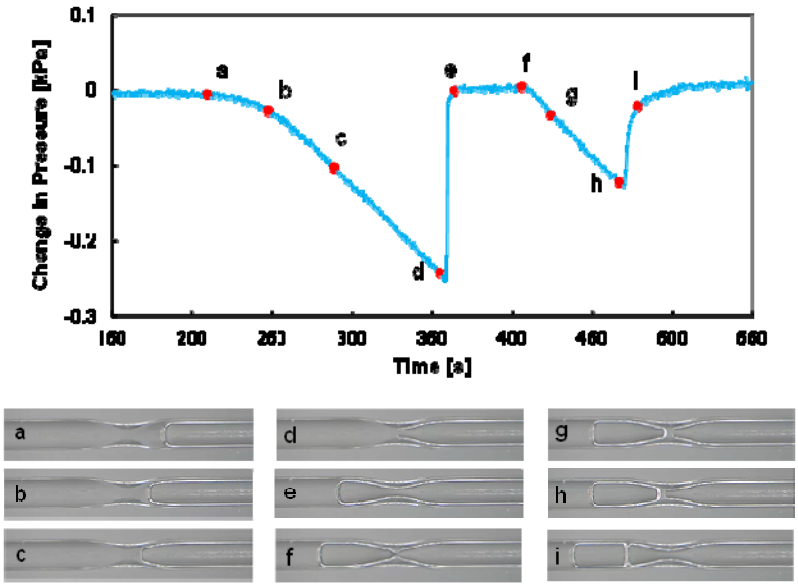

Figure 3. Characteristic pressure-time P-t signature and selected snapshots. Notice the formation of a liquid plug at the pore constriction leading to the generation of a second pressure pulse.

Hydrate Formation in Low Water Content Specimens

The experiment starts with water saturated bentonite specimen (wt = 200%, LL = 331%). The specimen was pressurized for 7 days before the temperature depression. No obvious hydrate crystal was observed in the specimen in the subsequent two days. The specimen was then put into a freezer. The pressure and temperature trajectory measured in the frozen process (Figure 4) demonstrates a press-sure increase upon temperature decrease in a closed system. This could on-

ly be explained by the formation of ice at the cost of hydrate dissociation, which releases gas into the chamber. In other words, ice is more stable than carbon dioxide hydrate in this experimental condition.

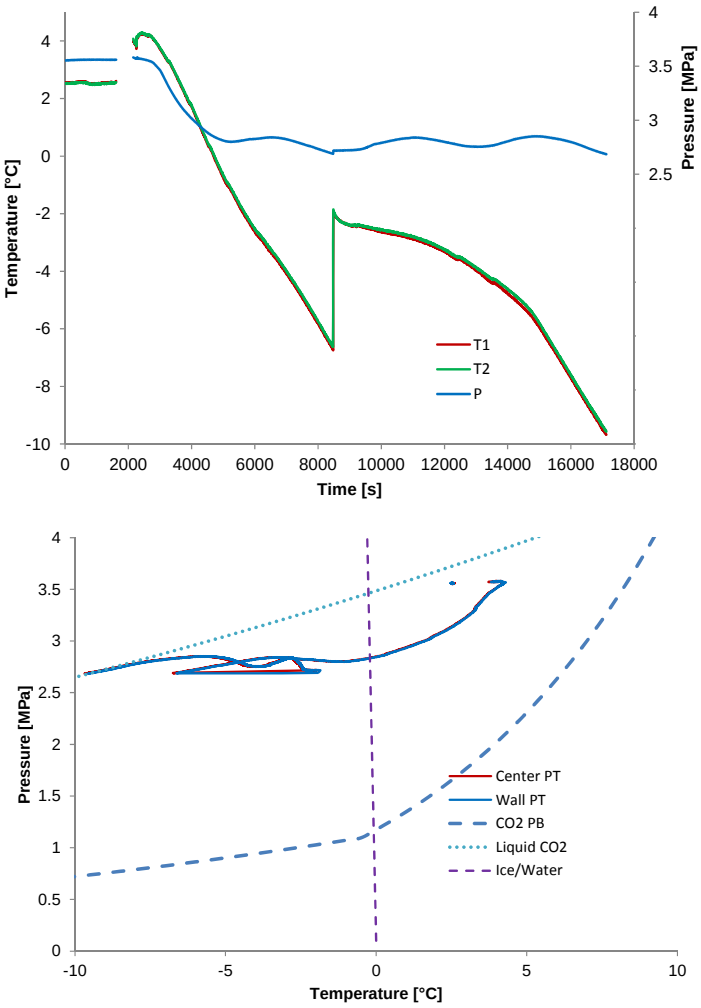

Figure 4. Pressure-temperature signatures during specimen frozen process.

The specimen then experienced a graduate temperature increase to facilitate the growth of hydrate. Resulted hydrate structure is illustrated in Figure 5. Fresh water released from melting ice was pulled towards the hydrate crystals in the upper space of the chamber. The distance between the crystal and the top of the specimen ranges from 7mm to 35mm. This result indicates the water transport by a thin layer of water film along the aluminum wall.

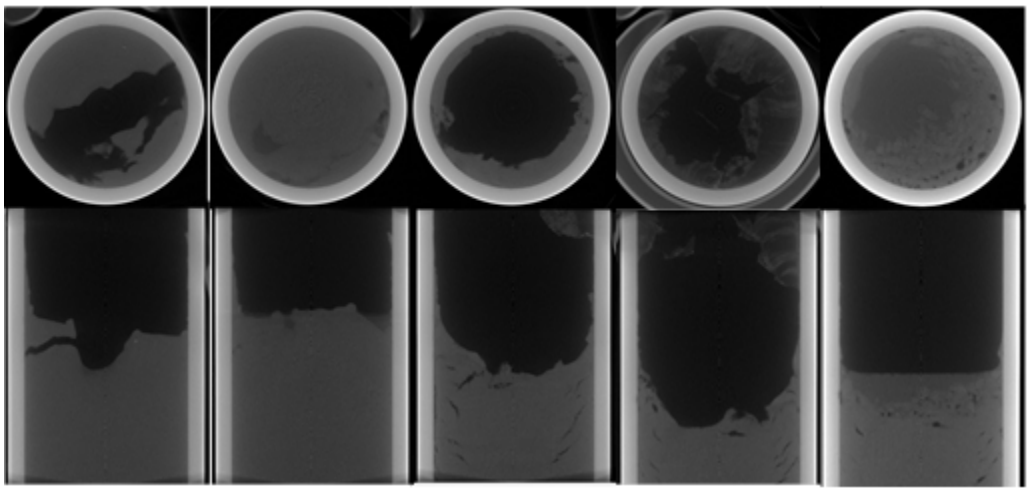

Figure 5: Comparison of specimen sections at different experimental stages. From left to right: initial condition, frozen condition, hydrate formation, same to previous, post-dissociation.

Flow Rate during Gas Production

Gas production by depressurization is analyzed. For a one dimension case where there is one hydrate lens buried inside the sediment, a production well is drilled parallel to the hydrate lens. The initial condition in the field is demonstrated as point A in Figure 6.a. Then the pressure in the production well is decreased to point C.

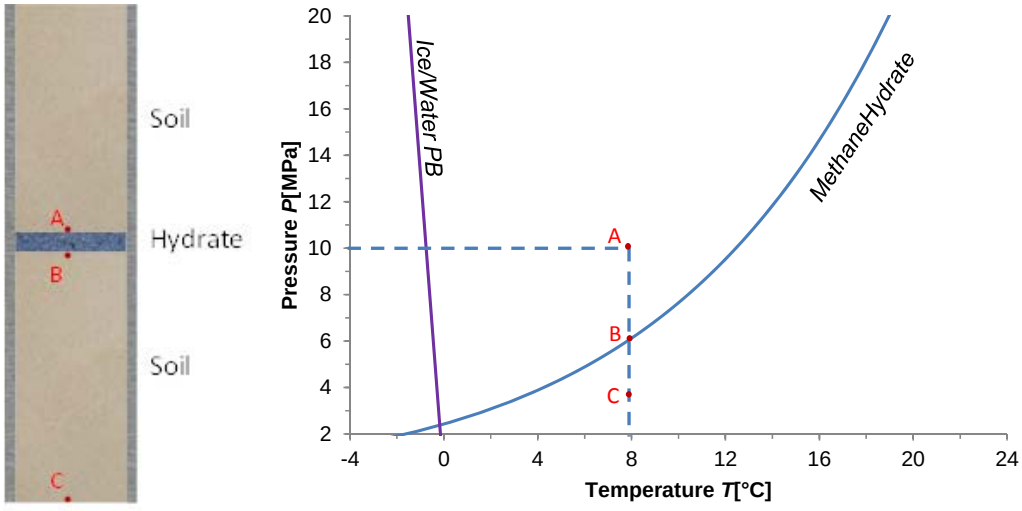

Figure 6: One-dimentional gas production analyses. Left: model illustration; Right: pressure-temperature conditions.

The field above point A maintains the initial condition. However, the geological condition between point B and point C is unknown, although the boundary condition is clear. The relationship between hydraulic conductivity and void ratio:

$$K = a \cdot S_s^{-1.9} \cdot e^b ,$$

where K is hydraulic conductivity in the unit of cm/s; a=1.5×10^{-5}cm/s; Ss is the specific surface of the sediments in the unit of m^2/g; e is the void ratio; b=3 for coarse-grained soils and b=3.9 for fine-grained soils. The relationship between void ratio and effective stress is obtained from consolidation curve:

$$e = e_0 - \lambda \cdot \ln\left(\frac{\sigma}{\sigma_0}\right),$$

$$\sigma = \sigma_0 \cdot \exp\left(\frac{e_0 - e}{\lambda}\right),$$

$$\mathrm{d}\sigma = \frac{-1}{\lambda} \cdot \sigma_0 \cdot \exp\left(\frac{e_0 - e}{\lambda}\right) \cdot \mathrm{d}e ,$$

where e_0 is the initial void ratio; λ is compression index; σ and σ_0 are effective stress and initial effective stress.

According to force equilibrium, the summation of pore fluid pressure and effective stress should be a constant:

$$\sigma + u = P ,$$

$$\mathrm{d}\sigma = -\mathrm{d}u ,$$

where u is the pore fluid pressure, and P is the total stress which is a constant.

Darcy's law gives the relationship between fluid pressure gradient and hydraulic conductivity:

$$q = K \cdot i = K \cdot \frac{1}{\rho \cdot g} \cdot \frac{\mathrm{d}u}{\mathrm{d}z} ,$$

where q is the flow rate, i is the water head gradient, ρ is the density, g is the standard gravity.

Therefore:

$$q = K \cdot i = a \cdot S_s^{-1.9} \cdot e^b \cdot \frac{1}{\rho \cdot g} \cdot \frac{1}{\lambda} \cdot \sigma_0 \cdot \exp\left(\frac{e_0 - e}{\lambda}\right) \cdot \frac{\mathrm{d}e}{\mathrm{d}z} .$$

Then:

$$\frac{q}{a \cdot S_s^{-1.9} \cdot \frac{1}{\rho \cdot g} \cdot \frac{1}{\lambda} \cdot \sigma_0 \exp\left(\frac{e_0}{\lambda}\right)} = e^b \cdot \exp\left(\frac{-e}{\lambda}\right) \cdot \frac{\mathrm{d}e}{\mathrm{d}z}.$$

Let:

$$C = \frac{q}{a \cdot S_s^{-1.9} \cdot \frac{1}{\rho \cdot g} \cdot \frac{1}{\lambda} \cdot \sigma_0 \exp\left(\frac{e_0}{\lambda}\right)}.$$

Then:

$$\frac{\mathrm{d}z}{\mathrm{d}e} = e^b \cdot \exp\left(\frac{-e}{\lambda}\right) \cdot \frac{1}{C},$$

$$z = \int e^b \cdot \exp\left(\frac{-e}{\lambda}\right) \cdot \frac{1}{C} \cdot \mathrm{d}e.$$

Figure 5 displays the result of one specific case.

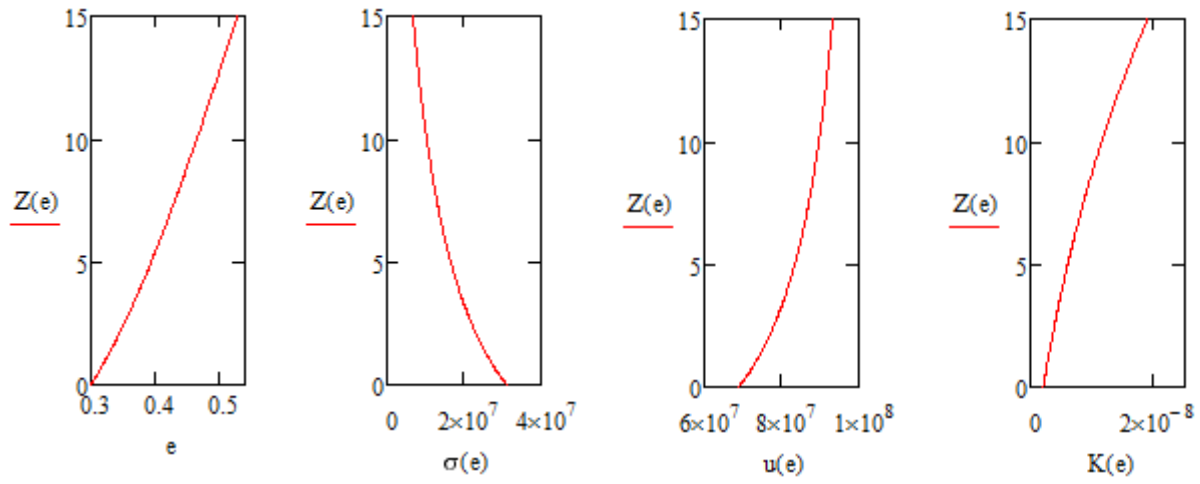

Figure 7: Geological parameters in the field between point B and point C. From left to right: void ratio, effective stress, pore fluid pressure, and hydraulic conductivity.

MILESTONE LOG

Milestone	Planed completion date	Actual completion date	Verification method	Comments
Literature review	5/2013	5/2013	Report	
Preliminary laboratory proto-col	8/2013	8/2013	Report (with preliminary val-idation data)	
Cells for Micro-CT	8/2013	8/2013	Report (with first images)	
Compilation of CT images: segregated hydrate in clayey sediments	8/2014	8/2014	Report (with images)	
Preliminary experimental studies on gas production	12/2014	12/2014	Report (with images)	
Analytical/numerical study of 2-media physical properties	5/2015	5/2015	Report (with analytical and numerical data)	
Experimental studies on gas production	12/2015	12/2015	Report (with data)	Additional studies in progress
Early numerical results related to gas production	5/2016	2/2016	Report	Additional studies in progress
Comprehensive results (in-cludes Implications)	9/2016	In progress	Comprehensive Report	

PRODUCTS

- **Publications & Presentations:**

  Jang, J. and Santamarina, J.C., 2016. Hydrate bearing clayey sediments: Formation and gas production concepts. *Marine and Petroleum Geology*, 77, pp.235-246.

- **Website:** Publications and key presentations are included in http://egel.kaust.edu.sa/ (for academic purposes only)
- **Technologies or techniques:** X-ray tomographer and X-ray transparent pressure vessel
- **Inventions, patent applications, and/or licenses:** None at this point.
- **Other products:** None at this point.

PARTICIPANTS & OTHER COLLABORATING ORGANIZATIONS

Research Team: The current team involves:

- Liang Lei (PhD student)
- Zhonghao Sun (PhD student)
- Jongchan Kim (PhD student)
- Sheng Dai (Assistant Professor)
- Carlos Santamarina (Professor)

Research Team:

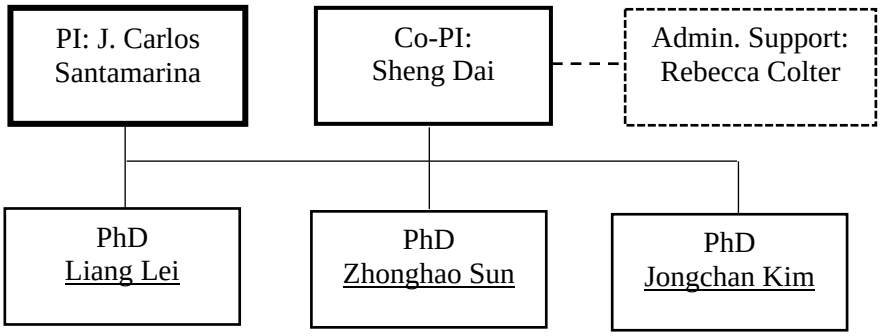

IMPACT

Understanding of fine grained hydrate-bearing sediments.

CHANGES/PROBLEMS:

No-cost time extension to 9/30/2017 has been requested.

SPECIAL REPORTING REQUIREMENTS:

We are progressing towards all goals for this project.

BUDGETARY INFORMATION:

As of the end of this research period, expenditures are summarized in the following table.

Note: in our academic cycle, higher expenditures typically take place during the summer quarter.

Baseline Reporting Quarter DE-FE009897	Budget Period 4							
	Q1		Q2		Q3		Q4	
	10/1/15 - 12/31/15		1/1/16 - 3/31/16		4/1/16 - 6/30/16		7/1/16 - 9/30/16	
	Q1	Cumulative Total	Q2	Cumulative Total	Q3	Cumulative Total	Q4	Cumulative Total
Baseline Cost Plan								
Federal Share	41,547	502,751	41,547	544,299	41,547	585,846	41,547	627,393
Non-Federal Share	11,935	146,969	11,935	158,904	11,935	170,839	11,935	182,774
Total Planned	53,482	649,720	53,482	703,203	53,482	756,685	53,482	810,167
Actual Incurred Cost								
Federal Share	22,802	461,960	32,381	494,341	45,285	539,627		
Non-Federal Share	15,167	152,445	10,111	162,556	5,056	167,612		
Total Incurred Costs	37,969	614,405	42,492	656,897	50,341	707,238		
Variance								
Federal Share	-18,745	-40,791	-9,166	-49,957	3,738	-46,219		
Non-Federal Share	3,232	5,476	-1,824	3,652	-6,879	-3,227		
Total Variance	-15,513	-35,315	-10,990	-46,305	-3,141	-49,447		

National Energy Technology Laboratory

626 Cochrans Mill Road
P.O. Box 10940
Pittsburgh, PA 15236-0940

3610 Collins Ferry Road
P.O. Box 880
Morgantown, WV 26507-0880

13131 Dairy Ashford Road, Suite 225
Sugar Land, TX 77478

1450 Queen Avenue SW
Albany, OR 97321-2198

Arctic Energy Office
420 L Street, Suite 305
Anchorage, AK 99501

Visit the NETL website at:
www.netl.doe.gov

Customer Service Line:
1-800-553-7681